

Analysing the Spectra of the Broad-Line Seyfert 1 Galaxy CBS 126

Chia-Ying Chiang^{1*}, R. C. Reis^{1,2}, A. C. Fabian¹, D. Grupe³ and S. Tsuruta⁴

¹*Institute of Astronomy, University of Cambridge, Madingley Road, Cambridge CB3 0HA*

²*Department of Astronomy, University of Michigan, Ann Arbor, MI 48109, USA*

³*Department of Astronomy and Astrophysics, Pennsylvania State University, 525 Davey Lab, University Park, PA 16802, USA*

⁴*Department of Physics, Montana State University, Bozeman, MT 59717, USA*

26 January 2023

ABSTRACT

We analysed the new simultaneous *Suzaku* and *Swift* data of the Broad Line Seyfert 1 (BLS1) galaxy CBS 126. A clear Fe emission line and an enormous soft excess are present in the source spectra. We fit the spectra with a relativistic reflection model and find the model tends to fit the data with a high iron abundance due to the large soft excess. By checking the difference and the RMS spectra, we find there is likely an absorption edge at ~ 0.89 keV, which might be caused by Oxygen or Neon. We also produced an analysis of the time-resolved spectra to examine the existence of the edge. Although a model with a high iron abundance is more desired in the time-resolved spectra, a model of solar iron abundance together with an absorption edge is a more physical explanation. Variation of the ionisation parameter in difference periods of spectra could be an alternative explanation of the excess seen in the difference spectra. We find the lack of low-energy (< 0.5 keV) data coverage in the time-resolved spectra to be the reason for the high iron abundance tendency. It is difficult to know if there are warm absorbers in this source from the current data. To further investigate the presence of warm absorbers and constrain the iron abundance, more detailed low-energy data are needed. The work presents that the spectra of a BLS1 can be explained by the standard reflection model.

Key words: accretion,

1 INTRODUCTION

Broad-line Seyfert 1 galaxies (BLS1s) are a subclass of Active Galactic Nuclei (AGN) with broad permitted optical emission lines ($H\beta$ FWHM ≥ 3000 km s⁻¹). Unlike narrow-line Seyfert 1 galaxies (NLS1s; $H\beta$ FWHM < 2000 km s⁻¹), the broad-line region (BLR) of a BLS1 is of high velocity and close to the central black hole. Studies of Boller et al. (1996) concluded that high-velocity and steep soft X-ray continuum slopes are not found in nature in AGN population. The steep, ultrasoft X-ray spectra in NLS1s are generally believed to be because of a relatively low-mass black hole with a very high accretion rate (Pounds et al. 1995) or distant BLR clouds (Puchnarewicz et al. 1992).

CBS 126 is a close ($z = 0.079$) broad line Seyfert 1 galaxy with $H\beta$ FWHM = 2980 ± 200 km s⁻¹ and a low Galactic absorption column ($N_H = 1.38 \times 10^{20}$ cm⁻², Dickey & Lockman). This AGN is part of the *ROSAT* AGN sample in Grupe et al. (1998a) and was found to be one of the AGNs with the highest degree of polarization (Grupe et al. 1998b). It was observed in X-rays during the *ROSAT* All-Sky Survey for 642s in 1990 but has not been observed by main missions such as *ASCA*, *XMM-Newton* and *Suzaku* until now. The source shows similar properties to NLS1s such as strong spectral

variability (see Fig. 1) and a large soft excess below ~ 1 keV, which are typical for NLS1s but unusual for BLS1s. CBS 126 does not harbour a low-mass black hole, and the mass of its central black hole is $\sim 7.6 \times 10^7 M_\odot$ (Shen et al. 2011, SDSS DR7 catalogue). This together with the high-velocity BLR clouds and the enormous soft excess arouse interest in this source.

The soft excess below ~ 1 keV in low-energy X-ray spectrum is commonly seen in AGNs. It is usually fitted by a blackbody with a temperature of $\sim 0.1 - 0.2$ keV, but the temperature of the component is fairly constant and not related to the luminosity and black hole mass of the source (Gierliński & Done 2004). Since the disc model predicts that the disc temperature should be correlated with the black hole mass, the soft excess is not likely to be due to the thermal emission from the accretion disc. Gierliński & Done (2004, 2006) suggested that soft excess can be caused by relativistically smeared and partially ionised absorption. However, an extreme outflow velocity is needed to produce a smooth spectrum (Schurch & Done 2007). Crummy et al. (2006) investigated a large sample of type 1 AGNs and found the relativistically blurred reflection model can reproduce the soft excess. The soft excess in the latter interpretation is in fact a series of blurred emission lines caused by disc reflection (Ross & Fabian 2005).

In this work we investigate the latest CBS 126 simultaneous *Suzaku* and *Swift* data set. The relativistic reflection model was

* E-mail: cychiang@ast.cam.ac.uk

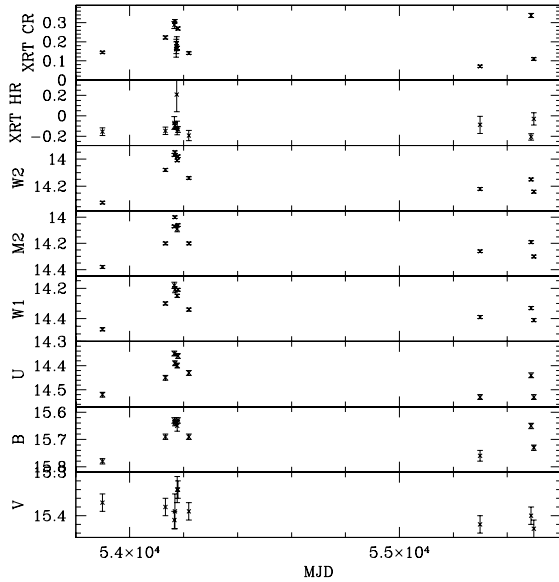


Figure 1. The figure shows the light curves of *Swift* instruments. The top two panels show the XRT count rate and hardness ratio, and the other panels show data extracted from different bands of UVOT data.

used to fit the spectra. We also produce the difference and the RMS spectra and find that an absorption edge is likely present. A time-resolved spectral analysis is also performed.

2 DATA REDUCTION

2.1 *Suzaku*

CBS 126 was observed by *Suzaku* in 2010 October for a total of ~ 200 ks of exposure time. The X-ray Imaging Spectrometer (XIS) was operated in the normal mode. All the detectors (XIS0, XIS1 and XIS3) were operated in both 3×3 and 5×5 editing modes. We reduced the data with the HEASOFT V6.10 software package following the *Suzaku* Data Reduction Guide. We used a circle with a 180 arcsec diameter to extract the source spectrum, and extracted the background spectrum using the same circular region. Response files were produced by the script XISRESP, which calls XISRMPGEN and XISSIMARFGEN automatically. Spectra of the three front-illuminated (FI) CCD XIS detectors (XIS0 and XIS3) were combined using the script addascaspec in FTOOL. The XIS 0.2–12.0 keV light curve of CBS 126 is shown in the upper panel in Fig. 2. It is clear that the XIS light curve is variable. We also produced the difference spectrum by subtracting the low-flux state spectrum from the high-flux state spectrum. The XIS light curve was divided into two flux intervals, both having a similar number of counts. The slice above the average count rate forms the high-flux state spectrum, while the slice below the average represents the low flux spectrum.

The Hard X-ray Detector (HXD) was operated in XIS-nominal pointing mode. The background spectrum of HXD/PIN consists of a non-X-ray background and a cosmic X-ray background. We obtained the non-X-ray background event file from a database of background observations made by the PIN diode. The cosmic X-ray background was estimated by model simulation using the PIN response for flat emission distribution. The source is

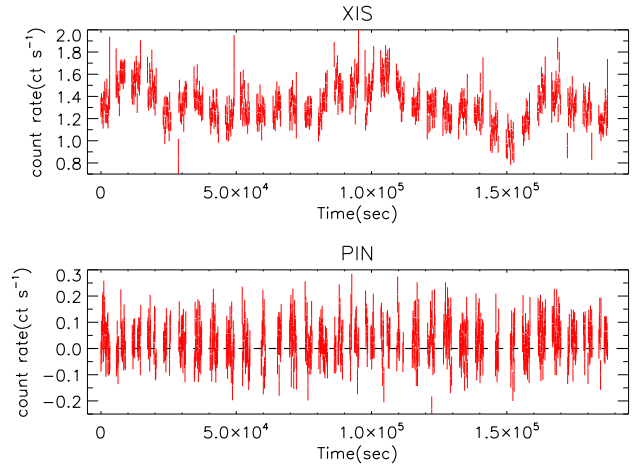


Figure 2. The figure shows the light curves of XIS and PIN data, with a time bin of 200s and 150s, respectively.

faint in the effective PIN energy band (14.0–45.0 keV), appearing at only 9% above the background level. Since the background dominates the PIN spectrum, we produced the earth-occulted background for a further check. Ideally the earth-occulted background should be identical to the non-X-ray background. The counts of the earth-occulted background are however slightly higher ($\sim 15\%$) than that of the non-X-ray background, which means the PIN data were mildly over-estimated. The navy blue points in Fig. 3 is the total background including the earth-occulted background and the cosmic background, and the cyan points slightly below stand for the PIN spectrum before background correction. It can be seen that if we replace the non-X-ray background with the earth-occulted background, PIN data are beyond detection. The green points in Fig. 3 are the background-corrected PIN data when using the non-X-ray background. We use only the PIN time-averaged spectrum in spectral fittings, as the data quality is not good enough to produce the time-resolved spectra. The light curve plotted in the lower panel of Fig. 2 also shows the source is faint in the PIN energy band, thus we did not generate a difference spectrum for PIN either.

2.2 *Swift*

We use *Swift* data taken simultaneously with the above *Suzaku* observation. Only the X-ray Telescope (XRT) data in Photon Counting mode were used, and all data were reduced following the standard procedure. The exposure time of this observation is about 6 ks. We extracted the source spectrum using a circle with a radius of $70''$, and the background spectrum was taken from an off source region with a radius of $200''$. The background region is much larger than the source region in order to get enough counts to model the background spectrum. The data were grouped to 20 counts s^{-1} , and fit between 0.3 and 5 keV. The difference spectrum was not generated because the exposure time is too short.

3 DATA ANALYSIS

We fit a powerlaw modified with Galactic absorption across the 0.9–4 keV and 7.5–12 keV energy ranges, and the results are shown in Fig. 3. An iron line is clearly shown in the *Suzaku* FI XIS spectrum in Fig. 3. It seems that no special features appear in the *Suzaku*

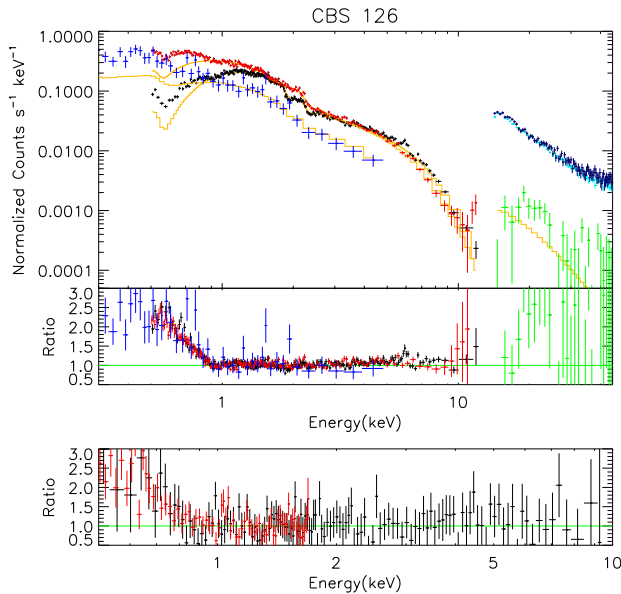


Figure 3. The upper part of the figure shows the overall spectra fitted with a powerlaw across 0.9 to 4 keV and 7.5 to 12 keV. The black data points are of the FI XIS spectrum, and red ones belong to the BI XIS spectrum. The PIN spectrum is presented by green points. The *Swift* XRT spectrum is shown using blue points. Navy blue and cyan points have been elaborated in section 2. Enormous soft excess at low energies and clear iron line structure can be clearly seen. The lower panel shows the data/model ratio of the difference spectra if the same modified powerlaw model is applied. The BI XIS difference spectrum above 1.7 keV and the FI XIS one above 10 keV are ignored because of bad quality.

back-illuminated (BI) XIS spectrum, and this may be because of the poor sensitivity of XIS1 in the high-energy band. A large soft excess that rises below ~ 0.9 keV is seen in both FI and BI XIS spectra and the *Swift* XRT spectrum. A Compton hump, which may be caused by reflection, appears in the *Suzaku* PIN energy band.

We also fit the modified powerlaw model to the *Suzaku* difference spectra (see the lower panel of Fig. 3). The difference spectra are quite noisy due to lack of data. A simple powerlaw fits the difference spectra above 1 keV, and it seems there are no features around the iron line band. Despite bad spectrum quality, soft excesses are shown as those seen in the real spectra. It is possible that there is another varying component in the low-energy band. A multiplicative component is likely as well, because contribution from such a component is not removed in the difference spectra even if it does not change with time.

3.1 Time-averaged Spectra

We try to fit the data with the simplest model that explains the iron line and the possible Compton hump. The model consists of a reflection continuum model REFLIONX (Ross & Fabian 2005) convolved by the KDBLUR model. We also model the neutral reflection with REFLIONX by setting the ionisation parameter $\xi = 1.0$. The Galactic absorption is modelled by TBnew using Wilms (Wilms et al. 2000) abundance. The model is called model A and the fitting parameters are shown in Table 1.

It is found that the iron abundance A_{Fe} tends to be higher than 9 times the solar value, which is not expected. If we set the iron

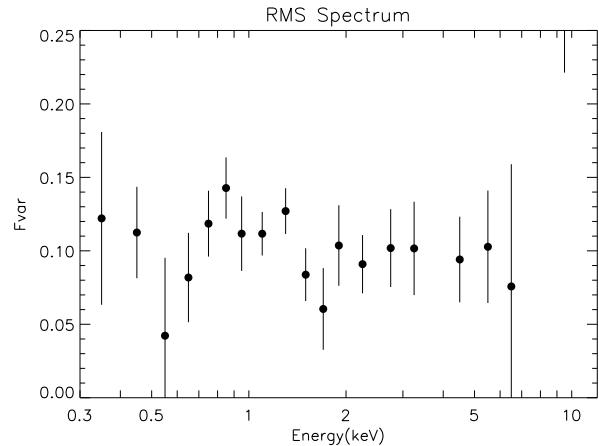


Figure 4. The figure shows the RMS spectrum of CBS 126. Each data point is calculated using a light curve with a time bin of 1ks. The last data point around 10 keV shows a much higher fraction of variability than the others because of noises around that energy band.

Table 1. The table below lists the fitting parameters and χ^2 obtained by models fitted over different energies. Γ is the photon index of the powerlaw component, and “index” stands for the emissivity profile index in the convolution model KDBLUR. In this table all the errors are at the 90% confidence level.

	Time-averaged		Time-resolved	
	Model A	Model B	Model A	Model B
Γ	2.01 ± 0.01	$2.16^{+0.01}_{-0.02}$	$2.00^{+0.02}_{-0.03}$	$2.11^{+0.03}_{-0.02}$
E_{edge}	-	0.89 ± 0.01	-	$0.88^{+0.02}_{-0.01}$
A_{Fe}	> 9.0	(1.0)	> 9.5	(1.0)
index	$7.2^{+0.8}_{-1.5}$	> 6.4	$4.2^{+0.3}_{-0.1}$	5.8 ± 2.1
$R_{\text{in}}(R_g)$	$3.0^{+0.6}_{-0.4}$	$1.7^{+0.3}_{-0.1}$	< 2.2	$1.7^{+0.5}_{-0.2}$
ϕ	$27^{+20}_{-5}^\circ$	$51^{+5}_{-8}^\circ$	$< 19^\circ$	$51^{+11}_{-16}^\circ$
$\chi^2/d.o.f.$	1767/1577	1762/1576	1148/1067	1181/1066

abundance to be the same as the solar value, the χ^2 of the fitting increases and the model failed to reproduce the soft excesses below 0.9 keV. A black-body component possibly arising from a low-temperature accretion disc was then considered, even though we do not expect the disc emission to change within such a short period of time and thus should not give rise to the soft excess seen in the difference spectrum. To examine whether the disc emission is present in the X-ray band and contributes variability, we generated the root mean square (RMS) spectrum using the technique developed by Edelson et al. (2002). The RMS spectrum of CBS 126 (see Fig. 4) is flat, and the variability of each energy band lies on a similar level. This implies that not a particular energy band contributes significantly more variability than the other energy bands. Therefore, the possibility of a black-body component can be ruled out, and a multiplicative component such as an absorption edge is a more appropriate assumption.

We added an absorption edge using ZEDGE to the model (hereafter model B) and fit the data again. The fitting improves considerably after including an absorption edge, and a lower χ^2 (reduced $\chi^2 = 1762/1576$) than the result of model A (reduced $\chi^2 = 1767/1577$) is obtained. Detailed fitting parameters obtained with model B are shown in Table 1. The energy of the absorption edge is ~ 0.89 keV,

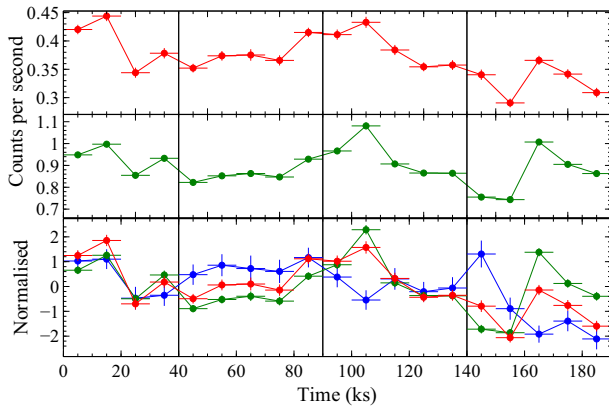


Figure 5. As describe in section 3.2, the figure shows the XIS light curve in different energies and the colour evolution (soft/hard is shown in blue). The red and green light curves describes the 0.3-1.0 keV and 1.0-10.0 keV respectively. In the lower panel these were normalized by dividing the difference between the count rate in each 10 ks bin and the mean count rate by the standard deviation.

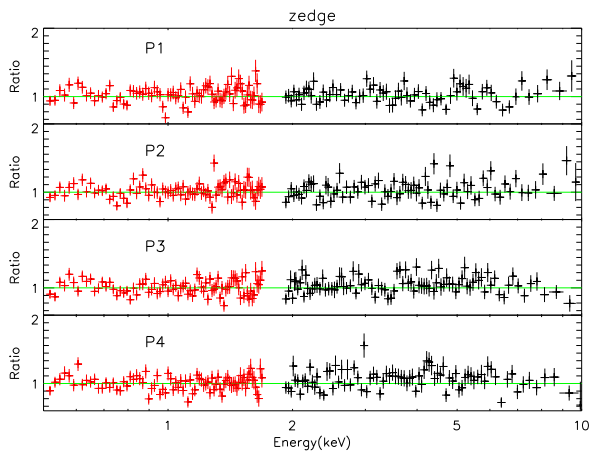


Figure 6. The figure shows the fitting results of spectra in different periods using model B. The black and red points represent FI and BI XIS data, respectively. The FI XIS spectra below 1.9 keV were ignored because the spectra turned to be noisy after breaking down into segments.

which is likely associated with Oxygen or Neon. It can be seen in Fig. 2 that the *Suzaku* XIS light curve is variable. If the absorption edge is a physical and reasonable explanation to the spectra, model B should fit the spectra in different periods with fixed ZEDGE parameters. To further investigate the presence of an absorption edge, we carry out an analysis on the time-resolved spectra.

3.2 Time-resolved Spectra

3.2.1 Spectral Fitting

A 0.3-1.0 keV and a 1.0-10.0 keV *Suzaku* XIS light curves with a 10 ks time bin were created and are shown in Fig. 5. The top two panels of Fig. 5 shows the “soft” (0.3-1.0 keV) and the “hard” (1.0-10.0 keV) light curves, respectively. The blue line in the lower panel shows the colour (the soft/hard ratio) evolution of the obser-

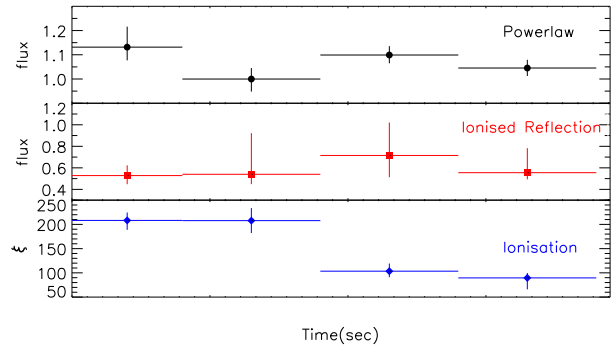


Figure 7. The figure shows, from top to bottom, the flux (in unit of 10^{-11} erg cm^{-2} s^{-1}) evolution of the powerlaw component, the ionised reflection component, and the evolution of the ionisation state. In this figure the error bars are of 1σ .

vation. When we look at the top two panels of Fig. 5, the count rates of the soft and the hard light curves seem to vary accordingly. The colour evolution curve, on the other hand, behaves in a different way. By observing the variations of the colour evolution curve, we noticed the presence of possibly four distinct periods and thus divided the observation into different segments and created a new set of time-resolved spectra. The observation was divided into four different segments as follows: 0-40 ks (period 1), 40-90 ks (period 2), 90-140 ks (period 3) and 140-190 ks (period 4). The resulting *Suzaku* FI XIS spectra are noisy in the low-energy band, therefore only the *Suzaku* low-energy BI XIS spectra were used. As mentioned in section 2, the *Suzaku* PIN spectrum is not of enough quality for further separation, so it is not included in time-resolved data analysis. The *Swift* XRT spectrum has an exposure time much less than 40 ks and is not suitable for time-resolving analysis.

We fit the time-resolved spectra with both model A and model B. Most of the fitting parameters are bound between the different periods of spectra. We let the normalisation of the powerlaw component, and the normalisation and the ionisation parameter of the ionised reflection component to vary. The normalisation of the neutral reflection component is free to vary, but tied between the periods (i.e. assumed to be constant at these time scales). When fitting with Model B, the parameters of ZEDGE are bound together because the absorption edge should not change in a short period of time. The fitting results of the time-resolved data are shown in Table 1. Fig. 6 displays the data/model ratio of the best-fitting results using model B, and spectra of different periods are shown in separate panels for clarity. It can be seen that model B fits spectra of difference periods well. The energy of the absorption edge is ~ 0.88 keV, which is consistent with that obtained by the time-averaged spectra. The existence of the absorption edge has been confirmed by the time-resolved spectra.

We find that model A, which still tends to give a high iron abundance, yields a better χ^2 in time-resolved spectra than model B does. This may be due to the lack of *Swift* spectra that offer a low energy coverage down to 0.3 keV. The resulting parameters of the time-resolved spectra are very similar to those obtained in the time-averaged spectra. The best-fitting values are not exactly the same but all agree within the 90% confidence level. The PIN data, the low-energy FI XIS spectrum, and the *Swift* XRT spectrum are not included in fittings of the time-resolved spectra, so slightly different best-fitting results of parameters are expected. Some parameters in the time-resolved spectra evolve with time, but it seems

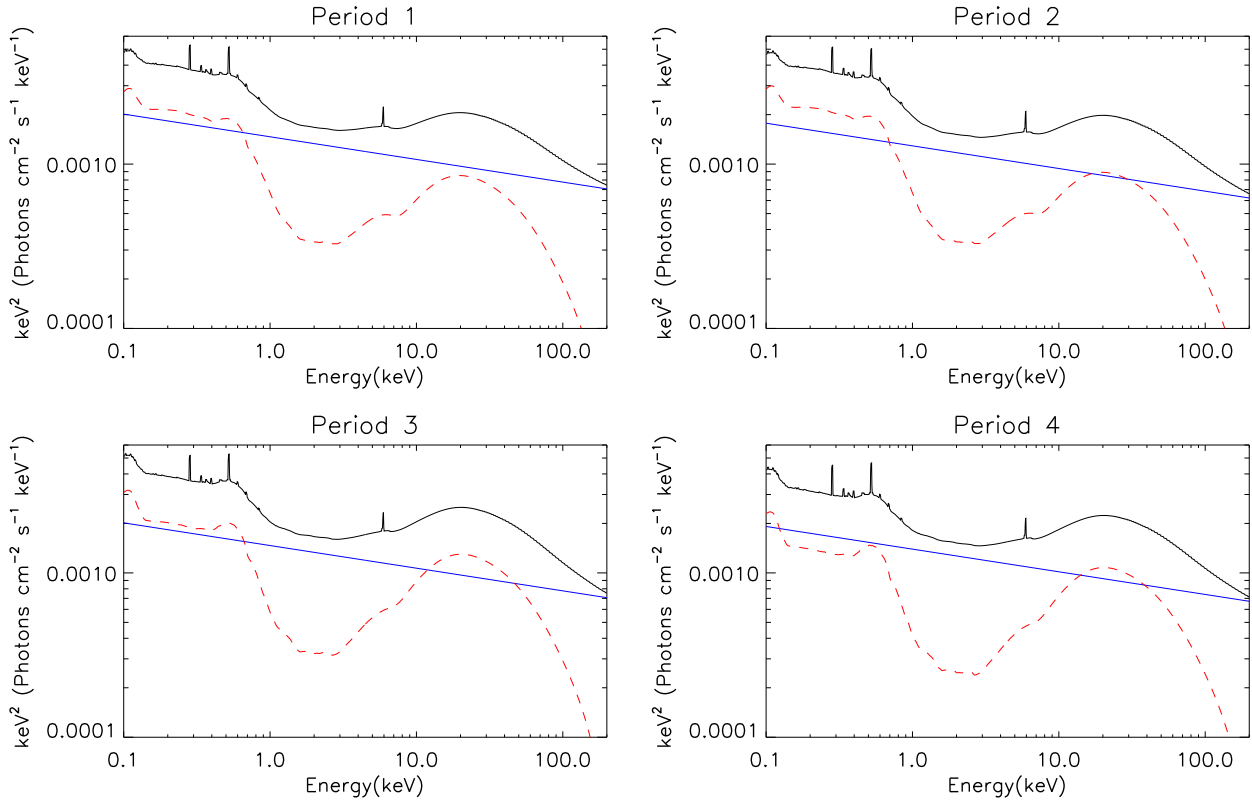


Figure 8. Each of the set of figures shows the decomposed components of model B in a period. The black line above shows the overall model without Galactic absorption and the edge. The blue line represents a $\Gamma = 2.11$ powerlaw. The red dash line shows the ionised reflection component. The neutral reflection component stays constant throughout the periods and is omitted for the purpose of clarity.

that properties such as photon index, emissivity index, inner radius of the accretion disc, and inclination angle remain nearly constant.

3.2.2 Flux Variation

The top two panels of Fig. 7 show the flux variation of the powerlaw and the ionised reflection components, and the lowest panel shows the variation of ionisation parameter of the reflection component. The ionisation parameter is defined as $\xi = L_{ion}/nR^2$, where L_{ion} is the ionising luminosity, n is the hydrogen number density, and R is the distance to the ionising source. ξ is proportional to the ionising luminosity, which is the intrinsic luminosity of the powerlaw continuum in this case. The flux of the powerlaw component varies with the light curve (see Fig. 5) as expected if the powerlaw is the main cause of variability in the source, while that of the ionised reflection component stays relatively constant in all periods. Nonetheless, the evolution of ionisation state does not follow the variation trend of the powerlaw component as expected from the $\xi = L_{ion}/nR^2$ definition of the ionisation parameter. Irrespective of which model is used, the ionisation parameter decreases with time. The highest ionisation parameter is found in period 1, while the lowest value in period 4. As the ionisation parameter falls, the soft emission below 1 keV drops.

We depict the evolution of the powerlaw and the reflection components in Fig. 8. As the neutral reflection component does not vary with time, we only plot the overall reflection (ionised plus neutral) component in the figure. From period 1 to period 2, the

reflection component stays constant but the powerlaw component drops a little. It looks like there are more soft excesses in period 2. In period 3 and period 4, the ionisation parameter drops and the soft excesses decrease.

Note that the difference in the soft excess between period 2 and 4 might also be a cause of the low-energy hump seen in the difference spectra. We try to fit the *Suzaku* difference spectra presented in Fig. 3 with an absorbed powerlaw and an ionised reflection component. The parameters of the reflection component were set the same as those obtained in the time-averaged spectral analysis. We find that the simple model fits the difference spectra well, indicating that the excess shown in the soft difference spectra could alternatively be caused by the change in the ionisation parameter.

4 DISCUSSION

4.1 High Iron Abundance or Absorption Edge

The iron abundance in a galaxy can be super-solar if star formation is ongoing in the galaxy. Some Seyfert I galaxies have super-solar abundances, for instance, 1H0707-495, which is a source that needs about eight times solar iron abundance to fit the spectra. There is a strong iron-K line and a sharp drop at ~ 7 keV in the spectra of 1H0707-495 (Fabian et al. 2009). The latter feature can be interpreted as the blue wing of the broad iron line, and this is the reason why a high iron abundance is required. Nevertheless, the iron-K in CBS 126 is not particularly strong, and there is no obvious drop or

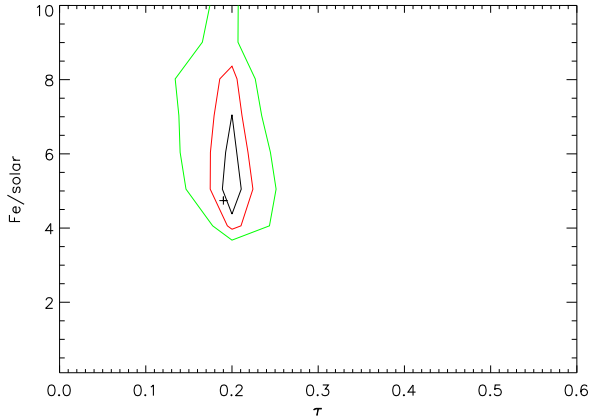


Figure 9. The figure shows the contour plot of the depth of the absorption edge against the iron abundance.

any special feature at that energy band. It is not very likely that the source has an intrinsic high iron abundance, thus the $A_{\text{Fe}} > 9$ result is not physical. In addition, it is difficult to explain the hump discovered in the low-energy difference spectra using model A, as the RMS spectrum implies there are no special components contributing extra variability in the low-energy band. The high value of iron abundance can be true if the entire difference spectra can be fitted with a simple modified powerlaw, but we found this unlikely.

Fig. 9 shows the contour plot of iron abundance against the depth of the absorption edge, and contours are plotted at 67%, 90% and 99% levels. The value of iron abundance spans a wide range from 3 to 10 in the contour plot, implying CBS 126 is likely super-solar, but the value of iron abundance is not constrained by the current dataset. We cannot make a correct measurement of the iron abundance yet.

Although the time-resolved spectra tend to be fitted with a high iron abundance, solar abundance plus an absorption edge is a more self-consistent explanation of the spectra. The low-energy data may be important in determining whether the source is super-solar or not. The *Swift* XRT spectrum is not of long exposure time, but the low-energy spectra are statistically stronger than the high-energy spectra. A few data points below 0.5 keV might change the model that the data favour. To test this we take the *Swift* XRT spectrum out in the time-averaged spectra, and we find the *Swift* data does play an important role. If we do not include *Swift* data, the dataset has no preference of the models (reduced $\chi^2 = 1720/1537$ for model A, and $1728/1534$ for model B). This implies that high-quality low-energy data may be essential to check the presence of absorption edge or constrain the iron abundance.

4.2 Possibility of the Existence of Warm Absorbers

Both the time-averaged and the time-resolved spectra can be fitted successfully by model B. The absorption edge has an energy of ~ 0.88 keV, close to the OVIII edge and a series of Neon absorption edges. The edge is possibly part of the absorption caused by a warm absorber. Moreover, it seems there is a weak absorption line at ~ 6.6 keV (see Fig. 10), which may be a Fe XXVI absorption line caused by a highly ionised warm absorber. This kind of warm absorber produces few absorption lines in the low-energy spectra. Therefore the absorption edge at ~ 0.88 keV is likely caused by a

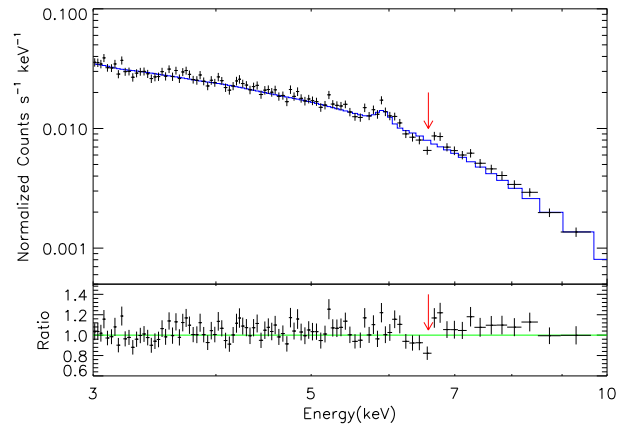


Figure 10. The figure shows the *Suzaku* FI XIS spectrum fitted with model B. The red arrow at ~ 6.6 keV in the figure indicates a possible Fe XXVI absorption line.

different warm absorber. However, the *Suzaku* XIS does not have enough energy resolution to confirm the existence of warm absorbers. The *Swift* XRT covers soft X-ray energies down to 0.3 keV but does not have enough energy resolution either. A more powerful instrument and an observation with a longer exposure time may be needed to confirm the assumption. Such an observation will also help index the absorption edge.

4.3 Variation of the Ionisation Parameter

CBS 126 shows enormous variability (see Fig. 1) in long-term X-ray observations, and it is also variable in short-term observations like the one that discussed in this paper. The time-resolved analysis indicates the ionisation parameter varies with time. The powerlaw component does not vary a lot during the observation, but the ionisation parameter drops significantly in period 3. In CBS 126 the powerlaw component does not vary dramatically, and it is likely that an increase in the hydrogen number density of the disc or the height of the corona caused the drop in $\xi = L_{\text{ion}}/nR^2$. The hydrogen number density of the disc is expected not to change a lot within a short period of time. The RMS spectrum indicates that the disc component does not contribute significant variability. It is more likely that the properties of the accretion disc remain constant. Assuming n remains constant, R increases a factor of ~ 1.4 between period 2 and 3.

As stated in section 3.2.2, different ionisation parameters produce different amount of soft excess. The excess at the soft X-ray band seen in the *Suzaku* difference spectra could simply be a result of changing ionisation parameter but not a multiplicative component. However, this again needs to be confirmed by a more detailed observation.

5 CONCLUSION

We test the relativistic reflection model on the new X-ray observation carried out in late 2010 of the BLS1 galaxy CBS 126. The spectra show enormous soft excesses in low-energy band, which are difficult to be explained by only the relativistic reflection continuum. An iron abundance larger than 9 times the solar value is

needed to produce the soft excesses. In Fig. 9 it seems the source is likely to be super-solar, but is not necessary as high as 9 times the solar value. Moreover, based on the information offered by the difference spectra and the RMS spectrum, a multiplicative component such as an absorption edge or a warm absorber is more likely. We find the model composed of a relativistic reflection continuum with solar abundance and an absorption edge fits the spectra better. To investigate this further, we carried out a time-resolved analysis to confirm the presence of this feature. Model B which contains an absorption edge and solar abundance fits the time-resolved spectra well. However, we find the lack of data below 0.5 keV causes a different model preference. The high-iron-abundance model A gives a better χ^2 in time-resolved analysis. We conclude that low-energy data below 0.5 keV are important to tell the differences between the models and constrain the value of iron abundance. In time-resolved analysis we find the ionisation parameter drops in period 3, and this is probably caused by an increase of the height of the corona. The change in ionisation parameter might also cause the excess at the low-energy band seen in the difference spectra.

This work shows that the reflection model can be used in interpreting the spectra of a BLS1 galaxy. We find the edge model explains both the time-averaged and the time-resolved spectra well, and it also interprets what we see in the difference and the RMS spectra. Nevertheless, due to the quality of the data, whether there are warm absorbers in the source and the exact value of iron abundance cannot be confirmed yet. The absorption edge is most likely an OVIII edge, but possibility of Neon cannot be ruled out. *Suzaku* and *Swift* do not have enough resolving power in the low-energy band. An observation by *Chandra* HETGS or *XMM-Newton* RGS may offer more details in the low-energy spectra and help constrain the iron abundance.

ACKNOWLEDGEMENTS

RCR is supported by NASA through the Einstein Fellowship Program, grant number PF1-120087. Swift at PSU is supported by NASA contract NAS5-00136. DG acknowledges support by NASA contract NNX07AH67G. ST is supported by NASA Grant NNX10AR32G.

REFERENCES

- Boller T., Brandt W. N., Fink H., 1996, *A&A*, 305, 53
 Crummy J., Fabian A. C., Gallo L., Ross R. R., 2006, *MNRAS*, 365, 1067
 Edelson R., Turner T. J., Pounds K., Vaughan S., Markowitz A., Marshall H., Dobbie P., Warwick R., 2002, *ApJ*, 568, 610
 Fabian A. C., Zoghbi A., Ross R. R., Uttley P., Gallo L. C., Brandt W. N., Blustin A. J., Boller T., Caballero-Garcia M. D., Larsson J., Miller J. M., Miniutti G., Ponti G., Reis R. C., Reynolds C. S., Tanaka Y., Young A. J., 2009, *Nature*, 459, 540
 Gierliński M., Done C., 2004, *MNRAS*, 349, L7
 —, 2006, *MNRAS*, 371, L16
 Grupe D., Beuermann K., Thomas H.-C., Mannheim K., Fink H. H., 1998a, *A&A*, 330, 25
 Grupe D., Wills B. J., Wills D., Beuermann K., 1998b, *A&A*, 333, 827
 Pounds K. A., Done C., Osborne J. P., 1995, *MNRAS*, 277, L5
 Puchnarewicz E. M., Mason K. O., Cordova F. A., Kartje J., Brabuardi A. A., Puchnarewicz E. M., Mason K. O., Cordova F. A., Kartje J., Branduardi-Raymont G., Mittaz J. P. D., Murdin P. G., Allington-Smith J., 1992, *MNRAS*, 256, 589
 Ross R. R., Fabian A. C., 2005, *MNRAS*, 358, 211
 Schurch N. J., Done C., 2007, *MNRAS*, 381, 1413
 Shen Y., Richards G. T., Strauss M. A., Hall P. B., Schneider D. P., Snedden S., Bizyaev D., Brewington H., Malanushenko V., Malanushenko E., Oravetz D., Pan K., Simmons A., 2011, *ApJS*, 194, 45
 Wilms J., Allen A., McCray R., 2000, *ApJ*, 542, 914